# Dopability of divalent tin containing phosphates for *p*-type transparent conductors

Tianshu Li,[1] Yawen Li,[1] M. Faizan,[1] Haowei Peng,[2,*] and Lijun Zhang[1,†]
[1]*State Key Laboratory of Superhard Materials, Key Laboratory of Automobile Materials of MOE, and College of Materials Science and Engineering, Jilin University, Changchun 130012, China*
[2]*Blue Bell, Pennsylvania 19422, United States*

(Received 19 April 2019; revised manuscript received 2 November 2019; published 30 December 2019)

Tin(II) containing phosphates, $Sn_nP_2O_{5+n}$ ($n$ is an integer), are promising candidates for *p*-type transparent conductors due to their good stability, suitable band gaps, and reasonable hole effective masses. Here we conduct first-principles calculations on $Sn_nP_2O_{5+n}$ type compounds by exploring their defect properties along with the dopability to find better candidates for *p*-type transparent conducting oxides. We consider two compounds, $Sn_3P_2O_8$ ($n = 3$) and $Sn_5P_2O_{10}$ ($n = 5$), with their binary counterpart SnO for a thorough comparison. Various likely native defects, as well as possible hydrogen-related extrinsic impurities have been examined. In $Sn_nP_2O_{5+n}$, Sn interstitial and Sn vacancy are the dominant donor and acceptor defects. In contrast to SnO, Sn vacancies have quite deep charge transition levels in $Sn_nP_2O_{5+n}$. The results indicate that both the studied phosphates are not good *p*-type transparent conductors even at the optimal growth conditions. However, our findings suggest that $Sn_nP_2O_{5+n}$ with a higher $n$ would allow for a relatively higher hole concentration and a shallow-level defect for Sn vacancy, thus calling future research in this direction.

DOI: 10.1103/PhysRevMaterials.3.124606

## I. INTRODUCTION

Transparent conducting oxides (TCOs) are highly needed in optoelectronic applications, such as solar cells [1–4], flat panel displays [5–7], and transparent electronics [8–10]. This can be attributed to their unique properties, more importantly, high optical transparency and low electrical resistivity. Currently, excellent *n*-type TCOs based on ZnO and other main group oxides have been commercially available. These binary oxides might be hard to apply as good *p*-type TCOs due to their localized O 2*p* character of the top valence bands. Such bands are often not dispersive enough for light hole effective mass which is needed for excellent hole conductivity, and also their energy is too low, thus preventing efficient *p*-type doping. To overcome both of these difficulties, an antibonding top valence band formed by *p*-*d* hybridization was proposed in $CuAlO_2$ as a prototype of *p*-type TCO [11]. The reported conductivity at room temperature of magnitude $0.95 \times 10^{-1}$ S cm$^{-1}$ is significantly smaller than the typical *n*-type TCOs like $SnO_2$ ($10^2$ S cm$^{-1}$) [12]. This situation also exists in other *p*-type TCOs, such as $CuM^{III}O_2$, $AgM^{III}O_2$ ($M^{III}$ = Sc, Cr, Co, Ga, In), and $SrCu_2O_2$ [13–17]. It has been observed experimentally that none of the above compounds has a hole conductivity higher than 10 S cm$^{-1}$. This may be due to the *d* orbital chemistry combined with the *p*-*d* coupling, and it is still a major challenge to design or discover novel *p*-type TCOs with optimum properties.

As an alternative to materials with *p*-*d* coupling, one could achieve the similar widened top valence bands by *s*-*p* antibonding. For instance, in the SnO where Sn possesses a valence state of +2, the valence band maximum (VBM) is mainly derived from O 2*p* and Sn 5*s* orbitals, with a fairly dispersive (in certain directions) and relatively high-energy valence band top. Such bands are favored for a light hole effective mass and feasible *p*-type dopability [18]. However, SnO possesses an anisotropic structure with undesirable anisotropic hole carrier transport. In addition to this, the high-quality film growth of SnO is still challenging [19–22].

Some other mixed-valence $Sn_xO_y$ have also been studied theoretically, including $Sn_2O_3$, $\alpha$-$Sn_3O_4$, $\beta$-$Sn_3O_4$, and $Sn_5O_6$ [23]. Among these, the two phases of $Sn_3O_4$ have suitable band gaps with relatively flat characters of the VBMs near the Fermi levels. Similarly, tin-based ternary oxides, like $Sn_2GeO_4$ [24] and $SnNb_2O_6$ [25], can be potentially used as effective *p*-type semiconductors due to their optimum band gaps or superior hole densities. Furthermore, some recent theoretical studies also demonstrated that the ternary compounds $K_2Sn_2O_3$ [26] and $MSn_2O_3$ (M = Sr, Ba) [27] can be promising candidates for *p*-type semiconductors. However, the above predictions are not justified fully and still need experimental verification. In the present work, we focus our attention on another group of Sn(II)-based compounds, the Sn phosphates (SnPOs) with the formula of $Sn_nP_2O_{5+n}$, which have been synthesized and tested experimentally [28–32]. Mercader *et al.* performed Mössbauer measurements on a well-characterized monoclinic crystal of $Sn_3P_2O_8$ at different temperatures as early as 1983 [33]. Fan *et al.* characterized the crystal structure of $Sn_5P_2O_{10}$ under hydrothermal conditions by reporting the triclinic space group along with other lattice parameters [34]. In a recent computational study, Xu *et al.* explored the electronic structures and optical properties of Sn(II) phosphates for optoelectronic applications [35]. The presence of Sn 5*s* states at the top valence bands implies the feasibility of *p*-type doping in SnPOs. In particular, they

*haoweipeng@gmail.com
†lijun_zhang@jlu.edu.cn

 

calculated the hole effective masses of $Sn_3P_2O_8$ ($2.55m_0$) and $Sn_5P_2O_{10}$ ($1.87m_0$) which are comparable to other widely studied $p$-type TCOs, e.g., $CuAlO_2$, with $m_h^* = 2.6m_0$ and $SrCu_2O_2$, with $m_h^* = 2.1m_0$ [26,36]. The band gaps calculated at HSE06 level are as high as 4.55 and 3.40 eV for $Sn_3P_2O_8$ and $Sn_5P_2O_{10}$, thus allowing high optical transparency. Such a combination of suitable band gap, low effective masses, and a good chemical stability suggests SnPOs as good candidates for highly efficient $p$-type TCOs.

A high-performance $p$-type TCO requires further research for achieving high holes concentration, which depends on shallow acceptor defects or the impurities contained therein. In this study, we aim to explore the intrinsic defect properties along with the formation energies and charge transition levels of SnO and $Sn_nP_2O_{5+n}$ using first-principles calculations. We will show that at certain growth conditions, a small but noticeable hole density can be obtained for $Sn_3P_2O_8$ and $Sn_5P_2O_{10}$. We will further explain the effect of hydrogen incorporation which occurs unintentionally during the synthesis and processing [37,38]. The chemical trend caused by increasing the integer $n$ suggests that high Sn-content in $Sn_nP_2O_{5+n}$ are potentially favorable for $p$-type TCOs and other optoelectronic applications.

## II. METHOD

We performed first-principles calculations within the framework of density-functional theory [39], as implemented in the Vienna Ab initio Simulation Package [40]. The interaction between core and valence electrons was explained using the frozen-core projector augmented wave pseudopotentials [40,41]. We used two exchange-correlation functionals: the Perdew-Burke-Ernzerhof (PBE) [42] functional for geometry optimization, and the Heyd-Scuseria-Ernzerh (HSE06) [43,44] density functional for electronic structures and defect formation energies (this has been carefully calibrated as discussed below). We used an original mixing parameter of 25% for the exact exchange in the HSE06 method. In our calculations for primitive cells, the kinetic energy cutoff for plane-wave basis was set to be 400 eV in conjunction with a grid spacing of $2\pi \times 0.03$ Å$^{-1}$ for Brillouin zone sampling. In supercell calculations, a $3 \times 3 \times 2$ supercell based on the 4-atom unit cell and a Monkhost $k$-mesh grid $3 \times 3 \times 3$ were used for SnO. For $Sn_3P_2O_8$ and $Sn_5P_2O_{10}$, only the $\Gamma$ point was used for the $1 \times 3 \times 1$ and $2 \times 2 \times 1$ supercells based on the 52-atom and 34-atom conventional unit cells.

The concentration of an intrinsic defect depends on the defect formation energy, $\Delta H_f$. For a point defect $D$ in the charge state $q$, its equilibrium concentration in a crystal is given by

$$c(D, q) = N_{\text{site}} g_q \exp[-\Delta H_f(D, q)/K_B T], \quad (1)$$

where $K_B$ is the Boltzmann constant, $T$ is the temperature, $\Delta H_f(D, q)$ is the formation energy, and $N_{\text{site}}$ is the number of possible sites for the defect. The degeneracy factor $g_q$ is equal to the number of possible structural configurations and electron occupancies. The formation energy and charge transition levels for a point defect can be expressed as follows:

$$\Delta H_f(D, q) = E(D, q) - E_h - \Sigma n_i\left(\Delta\mu_i + \mu_i^0\right) + q(\varepsilon_{\text{VBM}} + \varepsilon_f) + \Delta E_{\text{corr}}, \quad (2)$$

$$\varepsilon(q/q') = [\Delta H_f(D, q') - \Delta H_f(D, q)]/(q - q'). \quad (3)$$

where $E(D, q)$ is the total energy of the supercell containing a defect, $E_h$ is the total energy of the defect free supercell, $\Delta\mu_i$ is the chemical potential of the $i$th-atomic species relative to its ground-state elemental-phase chemical potential $\mu_i^0$, $n_i$ is the difference in the number of the $i$th-specie atoms between the defect and pristine supercells, $\varepsilon_{\text{VBM}}$ is the energy of VBM of the defect-free material, and $\varepsilon_f$ is the Fermi energy referenced to $\varepsilon_{\text{VBM}}$. The last term $\Delta E_{\text{corr}}$ corrects the error caused by the finite size of the supercell, including the image charge and potential alignment proposed by Lany and Zunger [45].

## III. RESULTS AND DISCUSSION

The optimized crystal structures of $Sn_3P_2O_8$, $Sn_5P_2O_{10}$, and SnO are shown in Figs. 1(a)–1(c). The SnO compound possesses tetragonal symmetry with spacegroup P4/nmm. The Sn atoms are located at the apex of square pyramids. The oxygen atoms are tetrahedrally bonded to Sn atoms having all the Sn-O bond distances equal to 2.25 Å [46]. The $Sn_3P_2O_8$ and $Sn_5P_2O_{10}$ are found to stabilize in the monoclinic and triclinic phases with space groups $P2_1/c$ and $P\bar{1}$, respectively. Both the compounds consist of trigonal-pyramidal $SnO_3$ and tetrahedral $PO_4$ networks. In these systems, the Sn atoms are surrounded by three O atoms, whereas the Sn $5s^2$ lone pair occupies each vertex of the tetrahedron. Two kinds of cation-centered groups are connected by sharing their vertices to form open frameworks with channels and cages [47]. The calculated formation enthalpies for $Sn_nP_2O_{5+n}$ with respect to binary counterparts SnO and $P_2O_5$ are $-220$ meV/atom ($Sn_3P_2O_8$) and $-190$ meV/atom ($Sn_5P_2O_{10}$), thus indicating high stabilities [35].

The calculated band structure diagrams for $Sn_3P_2O_8$, $Sn_5P_2O_{10}$, and SnO systems are shown in Figs. 1(d)–1(f), respectively. The orbital contributions of constituent elements are also plotted as color coded spheres. We can see from the plot that SnO possesses an indirect band-gap profile. The conduction band minimum (CBM) derived primarily from Sn $p$ states is located at the M-symmetry point, while the VBM which is derived mainly from O $2p$ states and Sn $5s$ states is found to occur at the $\Gamma$-symmetry line. In SnPOs, we find that both the compounds possess large band gaps, 4.43 eV for $Sn_3P_2O_8$ and 3.65 eV for $Sn_5P_2O_{10}$, which are well above the visible region of the spectrum. The Sn $5s$ states near the top of valence bands form antibonding states coupled with the phosphate atoms while the CBM is composed of Sn $5p$ states.

Defects and impurities in materials can take different forms including vacancies, antisites, self-interstitials, and substitutions. In SnPOs, the strong covalent bond in the $PO_4$ tetrahedra requires high energy to form P interstitials and antisite defects between O and P atoms. Sometimes it is rather difficult to generate antisite composed by Sn and P atoms in

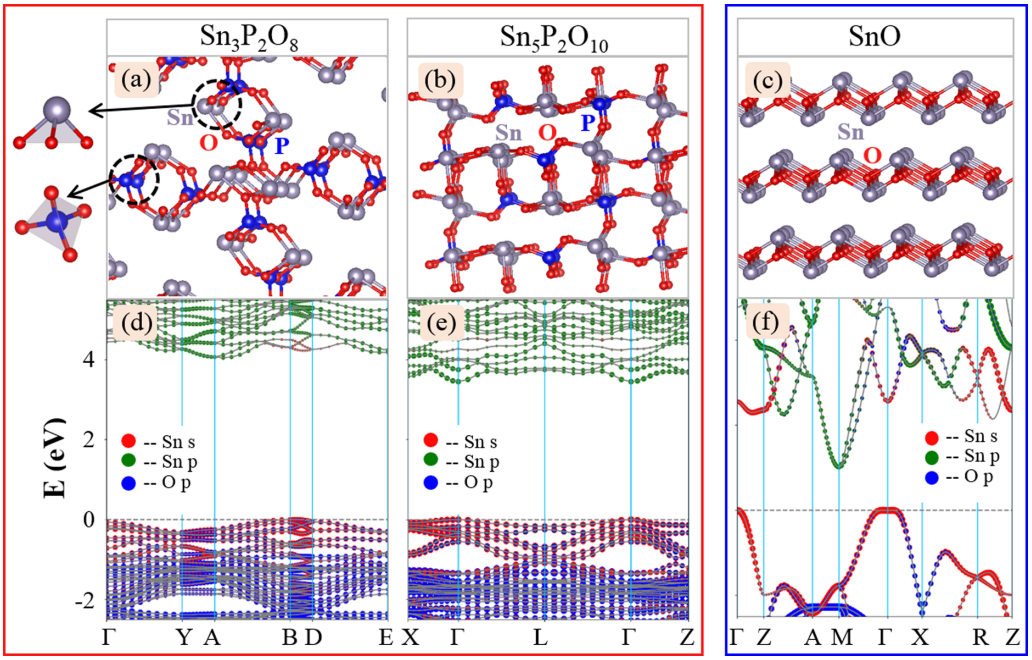


FIG. 1. [(a)–(c)] Crystal structures and the [(d)–(f)] orbital-projected band structures of $Sn_3P_2O_8$, $Sn_5P_2O_{10}$, and SnO, calculated at HSE06 level.

SnPOs as both the atoms are bonded with several O atoms. Here we mainly consider the following intrinsic defects in SnO and SnPOs, including three vacancies ($V_{Sn}$, $V_O$ and $V_P$), two antisites ($Sn_O$ and $O_{Sn}$), and three interstitials ($Sn_i$, $O_i$, and $P_i$).

We compared total energies of PBE functional for oxygen and tin vacancies at all possible vacancy sites. In both $Sn_3P_2O_8$ and $Sn_5P_2O_{10}$, the configuration of $V_O$ (with the lowest energy) is ∼0.05 eV lower than other configurations, while that of $V_{Sn}$ is ∼1.45 eV lower than others. For the interstitial defects, we found that $O_i$ is preferred to bond with multiple Sn atoms in SnPOs. We will only focus on the lowest-energy configurations of the selected compounds. The local structures of the lowest-energy configurations of $O_i$ and $Sn_i$ are shown in Fig. 2.

The PBE-optimized structures may lead to an inappropriate orbital hybridization between the defect states and band edge states mainly due to the band-gap underestimation [48]. To examine this, we performed supercell calculations with HSE06 functional in which we further optimized the $Sn_3P_2O_8$ having $V_{Sn}$ and $V_O$ vacancies and $O_i$ interstitial. The obtained results show slight changes up to 0.15 eV in formation energies and 0.08 eV in defect charge transition levels. Hence, using the PBE-optimized geometries would not affect the results obtained in this work.

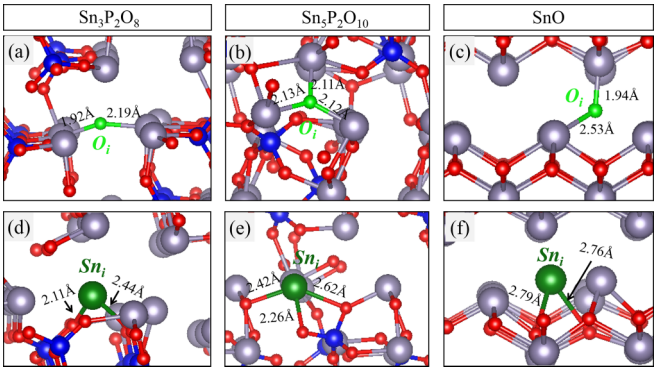


FIG. 2. Preferential locations of $O_i$ (light green) and $Sn_i$ (dark green) in the ground states of [(a) and (d)] $Sn_3P_2O_8$, [(b) and (e)] $Sn_5P_2O_{10}$, and [(c) and (f)] SnO. The bond length between interstitial and adjacent bonding atoms is indicated.

Besides the intrinsic defects, extensive studies have been performed showing the hydrogen incorporation both in crystalline and amorphous semiconductors [49–55]. One can easily incorporated hydrogen during the crystal growth as well as at any stage of the device processing. Therefore, we considered hydrogen as an extrinsic defect in the form of interstitials and their complex with vacancies to see what new features it can impart to the host materials.

Since the formation energy of a point defect depends on the chemical potentials of the constituent elements, we hereby performed a thorough evaluation of thermodynamic stability via the phase stability analysis. The stability diagrams for $Sn_3P_2O_8$, $Sn_5P_2O_{10}$, and SnO are shown in Fig. 3. We considered all the competing compounds documented in the Inorganic Crystal Structure Database [56,57]. In the case of SnO, the chemical potentials of the constituent elements are constrained by requiring SnO being thermodynamically stable by the following stability conditions,

$$\Delta\mu_{Sn} + \Delta\mu_O = \Delta H_f(SnO), \tag{4}$$

and avoiding the secondary phases:

$$\Delta\mu_{Sn} \leqslant 0, \tag{5}$$

$$\Delta\mu_O \leqslant 0, \tag{6}$$

$$\Delta\mu_{Sn} + 2\Delta\mu_O \leqslant \Delta H_f(SnO_2). \tag{7}$$

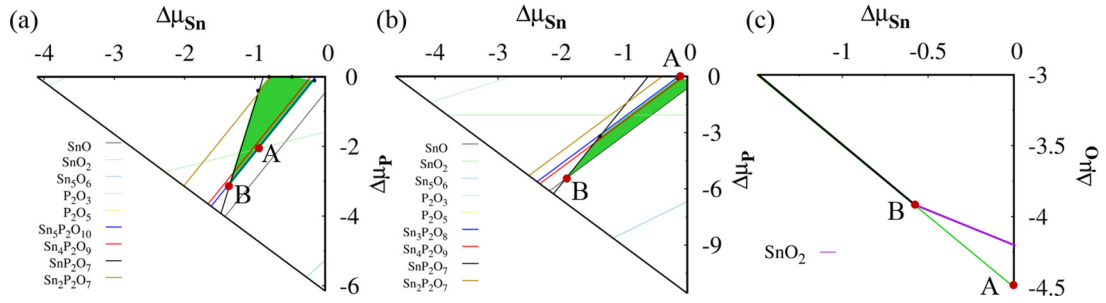


FIG. 3. The calculated phase diagrams of (a) $Sn_3P_2O_8$, (b) $Sn_5P_2O_{10}$, and (c) SnO, respectively. For ternary compounds, the green polygons indicate the stable regions. For binary compound, the green line indicates the stable region.

The Sn-rich/O-poor limit is defined by $\Delta\mu_{\mathrm{Sn}} = 0.0$ eV and $\Delta\mu_{\mathrm{O}} = \Delta H_f(\mathrm{SnO})$, whereas the Sn-poor limit can be defined from the formation energy of $SnO_2$ [58,59]. According to the formation energies of SnO and $SnO_2$ calculated with HSE06, $\Delta\mu_{\mathrm{Sn}}$ varies by an amount of 0.56 eV from the Sn-rich condition to the Sn-poor condition. Similarly, for SnPOs, the thermodynamic stability requires the following condition to fulfill:

$$m\Delta\mu_{\mathrm{Sn}} + n\Delta\mu_{\mathrm{P}} + k\Delta\mu_{\mathrm{O}} = \Delta H_f(\mathrm{Sn}_m\mathrm{P}_n\mathrm{O}_k), \qquad (8)$$

and the constraints related to elemental binary and ternary second phases:

$$x_i\Delta\mu_{\mathrm{Sn}} + y_i\Delta\mu_{\mathrm{P}} + z_i\Delta\mu_{\mathrm{O}} \leqslant \Delta H_f\left(\mathrm{Sn}_{x_i}\mathrm{P}_{y_i}\mathrm{O}_{z_i}\right), \quad i = 1, \ldots, Z, \qquad (9)$$

where $Z$ is the total number of competing phases. We calculated the values of $\Delta H_f$ for defects at two extreme points (A and B) that sampled the phase diagrams and made the $\Delta H_f$ of all neutrally charged defects positive in the respective compounds. For external impurities, we set $\mu_H (= \Delta\mu_H + \mu_H^0)$ equal to $\mu_H^0$, which is the energy of an H atom in the $H_2$ molecule at $T = 0$ K. We also considered competing hydrides but have not found any significant effect on $\Delta\mu_H$ under the Sn-rich growth conditions both in SnO and SnPOs, respectively.

The calculated formation energies of the intrinsic defects as a function of the Fermi level are plotted in Fig. 4. The oxygen interstitial is proved to be a deep acceptor for all the three compounds, with the $(0/2-)$ transition levels at 2.59, 2.40, and 0.99 eV above the VBM of $Sn_3P_2O_8$, $Sn_5P_2O_{10}$, and SnO. For the oxygen vacancy, the $(2+/0)$ transition levels of $V_{\mathrm{O}}$ are 3.44, 2.30, and 0.57 eV below the CBM of the respective compounds. As a result, $V_{\mathrm{O}}$ acts like a hole killer defect in the $p$-type condition with a Fermi level lower in energy than its charge transition level, while $O_i$ is an electron killer in the $n$-type condition with a Fermi level higher in energy than its charge transition level.

In SnO, $V_{\mathrm{Sn}}$ is a shallow acceptor with $\varepsilon(0/1-) = 0.04$ eV above the VBM, which is consistent with previous work of Varley *et al.* [37]. In SnPOs, $V_{\mathrm{Sn}}$ introduce relatively deep acceptor levels within the energy gaps, with $\varepsilon(0/2-) = 1.27$ eV and $\varepsilon(0/1-) = 0.55$ eV above the VBM in $Sn_3P_2O_8$ and $Sn_5P_2O_{10}$. As the Fermi level moves toward the CBM, $V_{\mathrm{Sn}}^{2-}$ is the first acceptor defect with a zero formation energy (automatically compensating electrons). This clearly defines the $n$-type Fermi level pinning. In $p$-type conditions, the value of $\Delta H_f$ for $V_{\mathrm{Sn}}^0$ is 1.1 and 0.5 eV higher than that of $O_i^0$ in $Sn_3P_2O_8$ and $Sn_5P_2O_{10}$, respectively.

The integer $n$ in the chemical formula of $Sn_nP_2O_{n+5}$ is the ratio of decomposition products SnO and $P_2O_5$. The similarity in the electronic structure of SnPOs and SnO should be dependent on the value of $n$. The above assumption is clearly supported by the fact that $V_{\mathrm{Sn}}$ is shallower in $Sn_5P_2O_{10}$ than that of $Sn_3P_2O_8$, as depicted in Fig. 4. To gain more insight into the electronic structure of SnPOs, we calculated the partial charge densities of the valence-band edge and plotted the results in Fig. 5. In SnO, the interaction of Sn $5s^2$ electrons with O $2p$ states in the valence band leads to form bonding and antibonding orbitals along with an active lone pair in the structure. Many studies have shown that a portion of Sn $5s$ states in the antibonding region are essential for producing active lone pairs [60–62]. This raises the valence band edge, resulting in an easy generation of shallow acceptor $V_{\mathrm{Sn}}$. The same scenario is seen in case of SnPOs [Figs. 5(a) and 5(b)] where a portion of O $2p$ states at the top valence bands is partially formed from $PO_4$ polyanions. The Sn $5s$ states hybridize with O $2p$ states forming bonding and antibonding orbitals and then Sn $5p$ states interact with antibonding orbitals. However, the fragile covalent bond between Sn and O in SnPOs weakens the bonding strength and lowers the energy of the antibonding states. Hence the acceptor levels of $V_{\mathrm{Sn}}$ in SnPOs are much deeper than those in SnO. Although the $V_{\mathrm{Sn}}$ in $Sn_5P_2O_{10}$ cannot be considered as a shallow acceptor, the defect transition level of $V_{\mathrm{Sn}}$ drops considerably by 0.72 eV when the integer $n$ changes from 3 to 5. Such a large drop in energy explicitly suggests Sn(II) phosphate with larger $n$ ($>5$) can potentially have a shallow-level $V_{\mathrm{Sn}}$, thus highlighting the need for further investigation.

We next consider the trends due to the Sn interstitials. The calculated $\varepsilon(1+/0)$ of $Sn_i$ is 0.78 eV below the CBM in case of SnO, and $\varepsilon(2+/0)$ of $Sn_i$ are 2.22 and 1.35 eV below the CBMs in $Sn_3P_2O_8$ and $Sn_5P_2O_{10}$, respectively (see Fig. 6). In SnO, the $\Delta H_f$ of $Sn_i$ is much higher than that of $V_{\mathrm{O}}$, which is also an $n$-type defect. In contrast, the $\Delta H_f$ of $Sn_i$ in SnPOs can be quite low, even negative for the $p$-type condition. The low $\Delta H_f$ of $Sn_i$ (as a native donor defect) is the main reason hindering SnPOs to be a high-efficiency $p$-type TCO. Even at the Sn-poor condition, the formation energy of $Sn_i^{2+}$ becomes zero when the Fermi level is 0.84 ($Sn_3P_2O_8$) and 0.52 eV ($Sn_5P_2O_{10}$) above the VBM. Such values explicitly define the

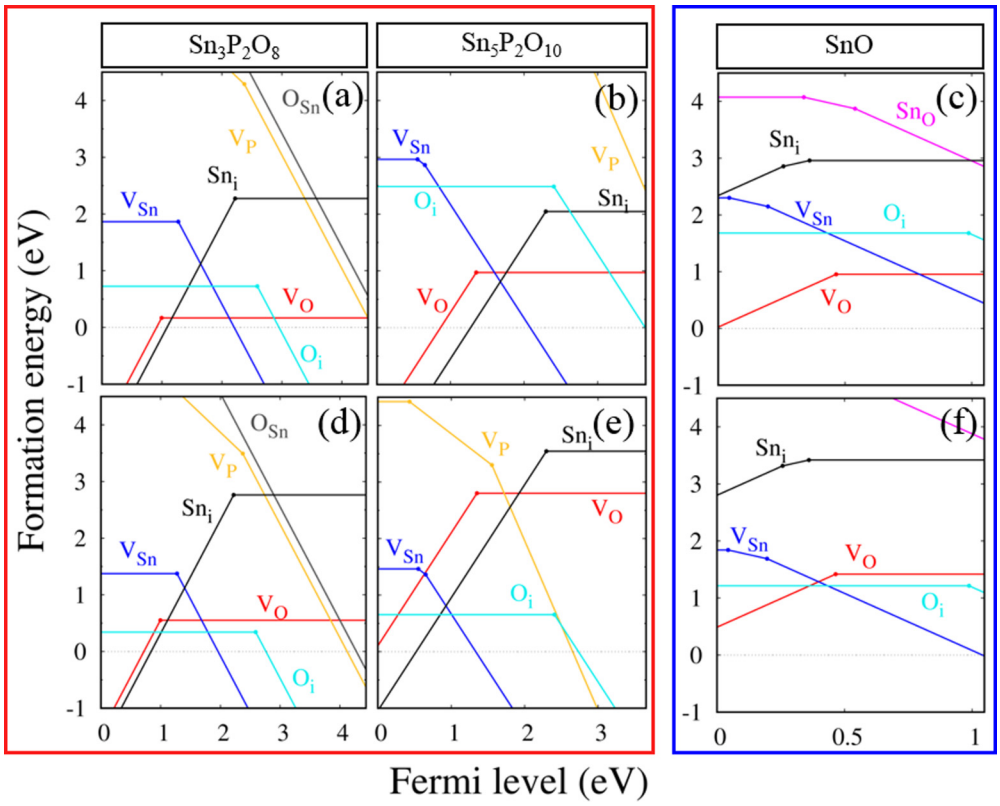


FIG. 4. The calculated formation energies of intrinsic defects in $Sn_3P_2O_8$, $Sn_5P_2O_{10}$, and SnO, as a function of $E_F$ under [(a)–(c)] Sn-rich and [(d)–(f)] Sn poor growth conditions. The slopes of line segments indicate the defect charge states and the kinks denote the charge transition levels. The Fermi levels are referenced to the VBM of respective host.

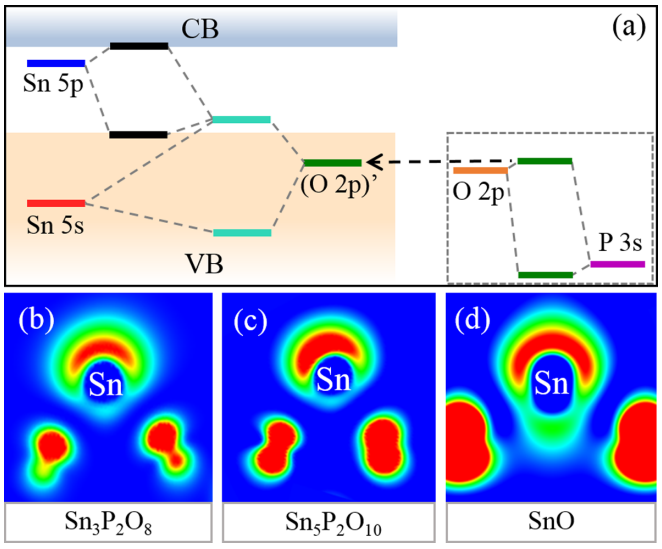


FIG. 5. (a) The schematic energy diagram for the band-edge states (especially the valence bands) formed by various atomic orbital states in SnPOs. The (O $2p$)′ state (dark green) refers to the "modified O $2p$ state," i.e., the antibonding state between O $2p$ and P $3s$ states. The areas of conduction bands (CB) and valence bands (VB) are shaded by blue and yellow, respectively. Band composed charge densities of top valence band with isosurface level of 0.01 for (b) $Sn_3P_2O_8$, (c) $Sn_5P_2O_{10}$, and (d) SnO.

$p$-type Fermi level pinning, i.e., the lower boundary of the Fermi level in these materials [63].

We observe that $V_{Sn}$ and $Sn_i$ are the two effective charged defects in the considered SnPOs. Both the defects respectively determine the $n$- and $p$-type Fermi level pinning, within the range of which the two dominant O-related defects will always be charge neutral.

The position of $E_F$ in a semiconductor is defined by the charge neutral condition,

$$p_0 + \sum\nolimits_{D,q} qc(D,q) = n_0, \tag{10}$$

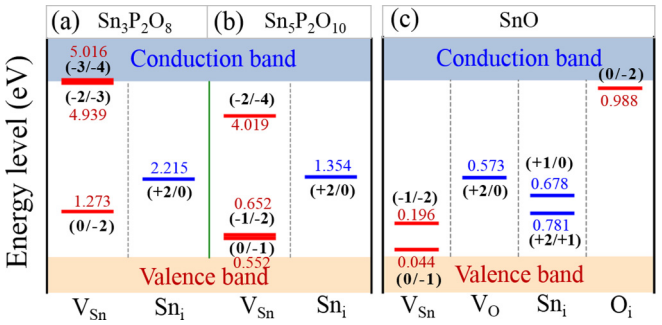


FIG. 6. The calculated charge transition levels for dominant donors (blue lines) and acceptors (red lines) in (a) $Sn_3P_2O_8$, (b) $Sn_5P_2O_{10}$, and (c) SnO. The values near the energy levels indicate energy differences between the charge transition levels and VBM (red color) or CBM (blue color).

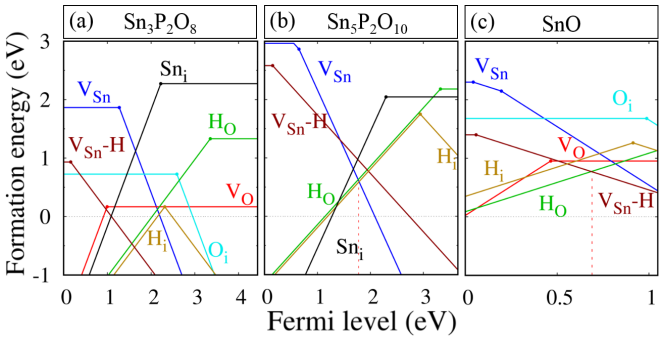


FIG. 7. The calculated formation energies of hydrogen-related and dominant intrinsic defects in (a) $Sn_3P_2O_8$, (b) $Sn_5P_2O_{10}$, and (c) SnO as a function of $E_F$ under Sn-rich growth conditions. The slopes of line segments indicate the defect charge states and kinks denote the charge transition levels. The Fermi level is taken as a reference to the VBM.

where $n_0$ and $p_0$ represent the free electron and hole densities. Assuming a growth temperature of 700 K under the Sn-poor condition [B points in Figs. 3(a) and 3(b)], the hole concentrations achieved at room temperature are $1.63 \times 10^{13}$ for $Sn_3P_2O_8$ and $3.26 \times 10^{15}$ $cm^{-3}$ for $Sn_5P_2O_{10}$, respectively. The corresponding Fermi levels are about 1.1 eV ($Sn_3P_2O_8$) and 0.8 eV ($Sn_5P_2O_{10}$) above the VBM. The free hole concentrations generated by the intrinsic defects are not high enough for an excellent $p$-type semiconductor, but the trend is quite encouraging. One may find superior hole concentrations and shallow $V_{Sn}$ defects in SnPOs with higher Sn contents.

The unintentional hydrogen incorporation can also lead to a more likely $p$-type conductivity in SnO [37]. Here we further explored the interaction of hydrogen with dominant defects in SnPOs and SnO systems. In hydrogen incorporation, we have considered three possible cases including its interaction with vacancies ($V_{Sn}$ and $V_O$) and single hydrogen interstitial ($H_i$). The Sn-rich growth conditions symbolized by points A in Fig. 3 were selected to calculate the formation energy of impurities in SnPOs and SnO. The formation energies versus Fermi level plots are shown in Fig. 7. In SnO, the $H_i$ acts as an amphoteric dopant with a transition level of $\varepsilon(1+/1-) = 0.92$, while its complex with $V_{Sn}$ ($V_{Sn}$-H) has a shallow level at 0.06 eV above the VBM. The low $\Delta H_f$ along with high binding energy (~1.92 eV) [37] suggests $V_{Sn}$-H in SnO is a potential source of $p$-type conductivity.

In SnPOs, when the H atom interacts with the $V_O$, the H atom prefers to sits at the center of the vacancy, successively forming a substitutional impurity $H_O$. Furthermore, in these systems, $H_O$ acts as donors with deep levels of 3.35 and 3.32 eV above the respective VBM, as shown in Figs. 7(a) and 7(b). The binding energies (defined by $\Delta H_f[V_{Sn}^{2-}] + \Delta H_f[H_i^+] - \Delta H_f[(V_{Sn}\text{-H})^-]$) calculated for the complex $V_{Sn}$-H in $Sn_3P_2O_8$ ($Sn_5P_2O_{10}$) is 0.97 eV (0.24 eV), and the corresponding transition level $\varepsilon(0/1-)$ is 0.16 eV (0.15 eV), above the VBM. Thus the complex acts like a shallow acceptor with high binding energy in $Sn_3P_2O_8$, but not stable enough in $Sn_5P_2O_{10}$. Like SnO, $H_i$ acts as an amphoteric impurity in both $Sn_3P_2O_8$ and $Sn_5P_2O_{10}$. The transition levels $\varepsilon(1+/1-)$ of $H_i$ are found to be 2.31 and 2.94 eV above the VBM of $Sn_3P_2O_8$ and $Sn_5P_2O_{10}$. In the extrinsic hydrogen incorporation under the Sn-rich growth condition, the Fermi level in $Sn_5P_2O_{10}$ can reach to 2.18 eV above the VBM. In comparison to the undoped $Sn_5P_2O_{10}$, the Fermi level moves toward the CBM by an amount of 0.16 eV. The above discussion clearly shows that hydrogen is not a suitable dopant in tin containing phosphates. For achieving $p$-type doping in SnPOs, the hydrogen incorporation should be suppressed in the synthesis.

## IV. CONCLUSIONS

In summary, we have systematically investigated the properties of intrinsic defects and extrinsic hydrogen impurities in tin containing phosphates $Sn_nP_2O_{5+n}$ for potential $p$-type TCOs. We considered two Sn(II) phosphates, $Sn_3P_2O_8$ and $Sn_5P_2O_{10}$, and compared the results with the binary SnO counterpart. The obtained results show important implication toward the tin monosulfide and divalent tin based ternary compounds with the Sn 5$s$ character at the top valence bands, such as $SnSO_4$. Calculations of different defect properties indicate that $V_{Sn}$ and $Sn_i$ are the most dominant native acceptor and donor defects in the studied compounds. The formation energies of these compounds determine the Fermi level pinnings. The oxygen vacancy and interstitial possess rather deep defect charge transition levels having low formation energies under specific growth conditions. However, they will always be charge inactive due to the allowed Fermi level positions of $V_{Sn}$ and $Sn_i$. In addition to this, the compounds show poor $p$-type behavior under Sn-poor growth condition. The defect ionization energy of Sn vacancies is found to decrease when the integer $n$ in $Sn_nP_2O_{5+n}$ changes from 3 to 5. All in all, the obtained results suggest that a better $p$-type conductivity can be achieved in $Sn_nP_2O_{5+n}$ with $n > 5$.

## ACKNOWLEDGMENTS

The authors acknowledge funding support from National Natural Science Foundation of China (Grants No. 61722403 and No. 11674121), Jilin Province Science and Technology Development Program (Grant No. 20190201016JC), Program for JLU Science and Technology Innovative Research Team (JLUSTIRT, 2017TD-03), and Graduate Innovation Fund of Jilin University (101832018C207). Calculations were performed in part at the high-performance computing center of Jilin University.

[1] A. Gupta and A. D. Compaan, Appl. Phys. Lett. **85**, 684 (2004).

[2] J. Muller, B. Rech, J. Springer, and M. Vanecek, Sol. Energy **77**, 917 (2004).

[3] F. A. Mahmoud and N. Ahmed, J. Semicond. **39**, 093002 (2018).
[4] T. Li, X. Zhao, D. Yang, M.-H. Du, and L. Zhang, Phys. Rev. Appl. **10**, 041001 (2018).
[5] Y.-H. Tak, K.-B. Kim, H.-G. Park, K.-H. Lee, and J.-L. Lee, Thin Solid Films **517**, 4490 (2009).
[6] M. Fahland, P. Karlsson, and C. Charton, Thin Solid Films **392**, 334 (2001).
[7] S.-H. K. Park, M. Ryu, C.-S. Hwang, S. Yang, C. Byun, J.-I. Lee, J. Shin, S. M. Yoon, H. Y. Chu, K. I. Cho, K. Lee, M. S. Oh, and S. Im, SID Symp. Dig. Techn. Pap. **39**, 629 (2008).
[8] K. Ravichandran and K. Thirumurugan, J. Mater. Sci. Technol. **30**, 97 (2014).
[9] S. Logothetidis, A. Laskarakis, S. Kassavetis, S. Lousinian, C. Gravalidis, and G. Kiriakidis, Thin Solid Films **516**, 1345 (2008).
[10] N. Kumar, B. Joshi, and K. Asokan, J. Semicond. **39**, 083002 (2018).
[11] H. Kawazoe, M. Yasukawa, H. Hyodo, M. Kurita, H. Yanagi, and H. Hosono, Nature **389**, 939 (1997).
[12] T. Isono, T. Fukuda, K. Nakagawa, R. Usui, R. Satoh, E. Morinaga, and Y. Mihara, J. Soc. Inf. Disp. **15**, 161 (2007).
[13] R. Nagarajan, N. Duan, M. K. Jayaraj, J. Li, K. A. Vanaja, A. Yokochi, A. Draeseke, J. Tate, and A. W. Sleight, Int. J. Inorg. Mater. **3**, 265 (2001).
[14] J. Tate, M. K. Jayaraj, A. D. Draeseke, T. Ulbrich, A. W. Sleight, K. A. Vanaja, R. Nagarajan, J. F. Wager, and R. L. Hoffman, Thin Solid Films **411**, 119 (2002).
[15] M. A. Marquardt, N. A. Ashmore, and D. P. Cann, Thin Solid Films **496**, 146 (2006).
[16] W. C. Sheets, E. S. Stampler, M. I. Bertoni, M. Sasaki, T. J. Marks, T. O. Mason, and K. R. Poeppelmeier, Inorg. Chem. **47**, 2696 (2008).
[17] A. Kudo, H. Yanagi, H. Hosono, and H. Kawazoe, Appl. Phys. Lett. **73**, 220 (1998).
[18] H. Hosono, Y. Ogo, H. Yanagi, and T. Kamiya, Electrochem. Solid State Lett. **14**, H13 (2011).
[19] E. Fortunato, R. Barros, P. Barquinha, V. Figueiredo, S.-H. K. Park, C.-S. Hwang, and R. Martins, Appl. Phys. Lett. **97**, 052105 (2010).
[20] Y. Ogo, H. Hiramatsu, K. Nomura, H. Yanagi, T. Kamiya, M. Hirano, and H. Hosono, Appl. Phys. Lett. **93**, 032113 (2008).
[21] J. A. Caraveo-Frescas, P. K. Nayak, H. A. Al-Jawhari, D. B. Granato, U. Schwingenschlögl, and H. N. Alshareef, ACS Nano **7**, 5160 (2013).
[22] Z. Wang, P. K. Nayak, J. A. Caraveo-Frescas, and H. N. Alshareef, Adv. Mater. **28**, 3831 (2016).
[23] J. Wang, N. Umezawa, and H. Hosono, Adv. Energy Mater. **6**, 1501190 (2016).
[24] J. Yu, J. Wang, M. Kumar, N. Umezawa, and H. Abe, J. Mater. Chem. C **6**, 11202 (2018).
[25] A. Samizo, N. Kikuchi, Y. Aiura, K. Nishio, and K. Mibu, Chem. Mater. **30**, 8221 (2018).
[26] G. Hautier, A. Miglio, G. Ceder, G.-M. Rignanese, and X. Gonze, Nat. Commun. **4**, 2292 (2013).
[27] Y. Li, D. J. Singh, M.-H. Du, Q. Xu, L. Zhang, W. Zheng, and Y. Ma, J. Mater. Chem. C **4**, 4592 (2016).
[28] M. Mathew, L. W. Schroeder, and T. H. Jordan, Acta. Crystallogr., Sect. B: Crystallogr. Cryst. Chem. **33**, 1812 (1977).
[29] E. Kim, D. Son, T. G. Kim, J. Cho, B. Park, K. S. Ryu, and S. H. Chang, Angew. Chem. Int. Edit. **43**, 5987 (2004).
[30] M. Behm and J. T. S. Irvine, Electrochim. Acta **47**, 1727 (2002).
[31] J.-G. Lee, D. Son, C. Kim, and B. Park, J. Power Sources **172**, 908 (2007).
[32] Y. W. Xiao, J. Y. Lee, A. S. Yu, and Z. L. Liu, J. Electrochem. Soc. **146**, 3623 (1999).
[33] R. C. Mercader, E. J. Baran, and A. R. López-García, J. Radiol. Nucl. Chem. Lett. **85**, 13 (1984).
[34] L.-Q. Fan, J.-H. Wu, and Y.-F. Huang, Z. Anorg. Allg. Chem. **634**, 534 (2008).
[35] Q. Xu, Y. Li, L. Zhang, W. Zheng, D. J. Singh, and Y. Ma, Chem. Mater. **29**, 2459 (2017).
[36] R. Gillen and J. Robertson, Phys. Rev. B **84**, 035125 (2011).
[37] J. B. Varley, A. Schleife, A. Janotti, and C. G. Van de Walle, Appl. Phys. Lett. **103**, 082118 (2013).
[38] B. Clerjaud, Physica B **170**, 383 (1991).
[39] P. Hohenberg and W. Kohn, Phys. Rev. **136**, B864 (1964).
[40] G. Kresse and J. Furthmüller, Phys. Rev. B **54**, 11169 (1996).
[41] P. E. Blöchl, Phys. Rev. B **50**, 17953 (1994).
[42] J. P. Perdew, K. Burke, and M. Ernzerhof, Phys. Rev. Lett. **77**, 3865 (1996).
[43] J. Heyd, G. E. Scuseria, and M. Ernzerhof, J. Chem. Phys. **118**, 8207 (2003).
[44] J. Paier, M. Marsman, K. Hummer, G. Kresse, I. C. Gerber, and J. G. Ángyán, J. Chem. Phys. **124**, 154709 (2006).
[45] S. Lany and A. Zunger, Phys. Rev. B **78**, 235104 (2008).
[46] I. Lefebvre, M. A. Szymanski, J. Olivier-Fourcade, and J. C. Jumas, Phys. Rev. B **58**, 1896 (1998).
[47] Y.-L. Liu, G.-S. Zhu, J.-S. Chen, L.-Y. Na, J. Hua, W.-Q. Pang, and R.-R. Xu, Inorg. Chem. **39**, 1820 (2000).
[48] A. Janotti, J. B. Varley, P. Rinke, N. Umezawa, G. Kresse, and C. G. Van de Walle, Phys. Rev. B **81**, 085212 (2010).
[49] S. K. Estreicher, Mater. Sci. Eng., R **14**, 319 (1995).
[50] J. I. Pankove and N. M. Johnson, *Hydrogen in Semiconductors: Hydrogen in Silicon* (Academic Press, New York, 1991).
[51] J. Neugebauer and C. G. Van de Walle, Phys. Rev. Lett. **75**, 4452 (1995).
[52] C. G. Van de Walle, Phys. Rev. B **56**, R10020 (1997).
[53] C. Kılıç and A. Zunger, Appl. Phys. Lett. **81**, 73 (2002).
[54] C. G. Van de Walle, Phys. Status Solidi B **235**, 89 (2003).
[55] C. G. V. d. Walle and J. Neugebauer, Annu. Rev. Mater. Res. **36**, 179 (2006).
[56] G. Bergerhoff, R. Hundt, R. Sievers, and I. D. Brown, J. Chem. Inf. Comput. Sci. **23**, 66 (1983).
[57] A. Belsky, M. Hellenbrandt, V. L. Karen, and P. Luksch, Acta Crystallogr. Sect. B **58**, 364 (2002).
[58] A. Togo, F. Oba, I. Tanaka, and K. Tatsumi, Phys. Rev. B **74**, 195128 (2006).
[59] J. P. Allen, D. O. Scanlon, L. F. J. Piper, and G. W. Watson, J. Mater. Chem. C **1**, 8194 (2013).
[60] A. Walsh and G. W. Watson, Phys. Rev. B **70**, 235114 (2004).
[61] A. Walsh and G. W. Watson, J. Phys. Chem. B **109**, 18868 (2005).
[62] A. Walsh, D. J. Payne, R. G. Egdell, and G. W. Watson, Chem. Soc. Rev. **40**, 4455 (2011).
[63] S. B. Zhang, S.-H. Wei, and A. Zunger, J. Appl. Phys. **83**, 3192 (1998).